Earthquake Science
地震学报英文版 ISSN 1674-4519 CN 11-5695/P

Foreshocks of the 2016 M_S5.1 Yunlong earthquake in Western Yunnan, China, and implications for earthquake nucleation

Gaohua Zhu, Hongfeng Yang, Yingying Zhang

Citation: Zhu GH, Yang HF, Zhang YY (2025). Foreshocks of the 2016 $_S$5.1 Yunlong earthquake in Western Yunnan, China, and implications for earthquake nucleation. *Earthquake Science*, **38**(0): 1–11, doi:

View online:

Earthquake Science 38 (2025) 1–11

Contents lists available at ScienceDirect

Earthquake Science

Journal homepage: https://www.keaipublishing.com/en/journals/earthquake-science/

Foreshocks of the 2016 M_S5.1 Yunlong earthquake in Western Yunnan, China, and implications for earthquake nucleation

Gaohua Zhu[1,2], Hongfeng Yang[3,✉] and Yingying Zhang[4]

[1] *Key Laboratory of Ocean Observation and Forecasting*, *Institute of Oceanology*, *Chinese Academy of Sciences*, *Qingdao* 266071, *China*
[2] *Laboratory for Marine Geology*, *Qingdao Marine Science and Technology Center*, *Qingdao* 266237, *China*
[3] *Department of Earth and Environmental Science*, *Faculty of Science*, *The Chinese University of Hong Kong*, *Shatin*, *Hong Kong* 999077, *China*
[4] *China Earthquake Networks Center*, *Beijing* 100045, *China*

Key points:

- We detect and locate 343 foreshocks of the 2016 M_S5.1 Yunlong earthquake using the matched filter detection.
- The spatiotemporal evolution of the foreshocks indicates that the nucleation of the 2016 M_S5.1 Yunlong earthquake was prominently governed by stress perturbation.
- The temporal changes in *b* values reveal precursory drops before the Yangbi mainshocks in the adjacent area.

A B S T R A C T

Monitoring the evolution of foreshocks can be a valuable way to analyze the nucleation process. Foreshocks accompanying moderate mainshocks have been recorded in the west of Yunnan Province, China. We obtain the earthquake catalog and source parameters of the 2016 Yunlong foreshocks, and discuss the implications for the nucleation processes of the earthquake in western Yunnan, China. By using the matched filter detection, we identify 343 foreshocks with a magnitude of −0.8−4.5, starting with a magnitude 1.0 foreshock approximately 3 months before the 2016 M_S5.1 Yunlong mainshock. The spatial distribution of foreshocks doesn't show localization or directional migration towards the mainshock. Coulomb stress analysis suggests a positive stress perturbation at the mainshock nucleate area. These observations indicate a cascade-triggering mechanism of the 2016 Yunlong earthquakes. We further collect published catalogs of 2021 Yangbi and 2017 Yangbi foreshocks in the adjacent area, and analyze the temporal changes in *b* values. The temporal changes in *b* values reveal precursory drops before the mainshocks.

Production and Hosting by Elsevier on behalf of KeAI

Peer review under the responsibility of Institute of Geophysics, China Earthquake Administration.

✉ **Corresponding author.** Yang HF, email: hyang@cuhk.edu.hk

Article history:

https://doi.org/

Keywords: foreshocks; Yunlong mainshock; earthquake detection and location

Citation: Zhu GH, Yang HF and Zhang YY (2025). Foreshocks of the 2016 M_S5.1 Yunlong earthquake in Western Yunnan, China, and implications for earthquake nucleation. Earthq Sci **38**, doi:

1. Introduction

Earthquake prediction is extremely challenging but of great significance to the society. The 1975 *M*7.3 Haicheng earthquake that occurred in northeast China is considered the only major earthquake known to have been predicted (Scholz, 1977; Wang KL et al., 2006). Official predictions were made and evacuation measures were taken for civil protection (Wang KL et al., 2006). Anomalies before the Haicheng earthquake were documented, such as changes in geodetic deformation, gravity, groundwater level and color, and peculiar animal behavior (Chen YT et al., 1980; Jin AS and Aki, 1986). The most important precursor was an intense foreshock sequence (Jones et al., 1983; Xu SX et al., 1982), which triggered the final prediction. The successful prediction of the Haicheng earthquake motivates people to investigate earthquake processes and pursue the goal of earthquake prediction.

Studying foreshocks may shed light on the goals. Yet intriguing discussions about the physical mechanisms of the earthquake nucleation process have been in long debate (Cattania and Segall, 2021; Ellsworth, 2019; Huang H et al., 2020). The pre-slip model proposes that aseismic slip occurring at the mainshock hypocenter can generate foreshocks during the mainshock nucleation (Bouchon et al., 2011; Kato and Nakagawa, 2014; Kato et al., 2012; Tape et al., 2018). During pre-slip processes, foreshocks could be interpreted as byproducts of the nucleation process of a large event, driven by pre-seismic slip, which is optimistic for short-term prediction (deterministic process) (Ellsworth, 2019). In comparison, the cascade triggering mechanism suggests that foreshocks are triggered by stress perturbations of previous earthquakes instead of aseismic slip (Ellsworth and Bulut, 2018; Mori, 1996; Yoon et al., 2019; Zhu GH et al., 2022). Therefore, foreshocks may not be different from other smaller earthquakes (stochastic process), which implies that the magnitude of the earthquake is unknown until the rupture stops (Abercrombie and Mori, 1996; Ellsworth, 2019). Besides, fluids and possible attendant aseismic slip may also play important roles in the earthquake nucleation process (e.g. Lei XL et al., 2024; Liu M et al., 2023; Peng ZG et al., 2024). During the fluid-triggered seismic process, possible along-strike or along-dip triggered front of seismicity accords with a parabola proportional to the square root of time (Shapiro et al., 1997).

In addition to the physical mechanisms of foreshocks, the statistical features of foreshocks are also elusive. A critical unknown in real-time earthquake risk evaluation during an ongoing seismic sequence is whether the mainshock has already happened or is yet to come. Monitoring *b* values of the Gutenberg-Richter law in real-time may shed light on the vital issue (Gulia and Wiemer, 2019). The cumulative number (*N*) of earthquakes is larger or equal to magnitude (*M*) as $\log(N) = a - bM$, where *a* value represents activity rate, and *b* value describes the earthquake-size distribution (Gutenberg and Richter, 1944). The *b* value is regarded as an indicator of differential stress (Schorlemmer et al., 2005). A systematic *b* value reduction before the main event has been proposed in laboratory observations (Scholz, 1968; Goebel et al., 2013). Retrospectively, obvious drops in *b*-values relative to background values before large natural events were established as a traffic-light system for earthquake warnings (Gulia and Wiemer, 2019). However, the tests using well-recorded earthquake foreshock sequences in Ridgecrest, California, and Maria Antonia, Puerto Rico show ambiguous warning levels, suggesting that such *b* value based real-time warning values depend strongly on dense instrumentation, high completeness catalog and expert judgment (Dascher-Cousineau et al., 2020). Therefore, further testing of the effectiveness of precursory drop in *b* values in different geological environments is necessary.

Foreshocks proceeding moderate mainshocks have been recorded in the west of Yunnan Province, China, such as the May 17, 2016 M_S5.1Yunlong and 2021 M_S6.4 Yangbi (Figure 1b) earthquake sequences. These earthquakes occurred on the southwest side of Weixi-Qiaohou-Weishan fault. The Weixi-Qiaohou-Weishan fault is caused by the northward extension of the Red River Fault (Figure 1). The seismic observations in western Yunnan provide a great opportunity to study spatial-temporal evolution of foreshocks and time-varying *b* values. The foreshocks of the 2021 Yangbi M_S6.4 mainshock have been investigated in recent studies (He X et al., 2023; Lei XL et al., 2021; Liu M et al., 2022; Zhang YY et al., 2022; Zhou YJ et al., 2022; Zhu GH et al., 2022), suggesting a dominant cascade triggering mechanism in the 2021 Yangbi sequence, but the inconsistency is whether aseismic slip exists at the initial stage. The Yunlong M_S5.1 earthquake occurred on May 17, 2016 (Figure 2), and was

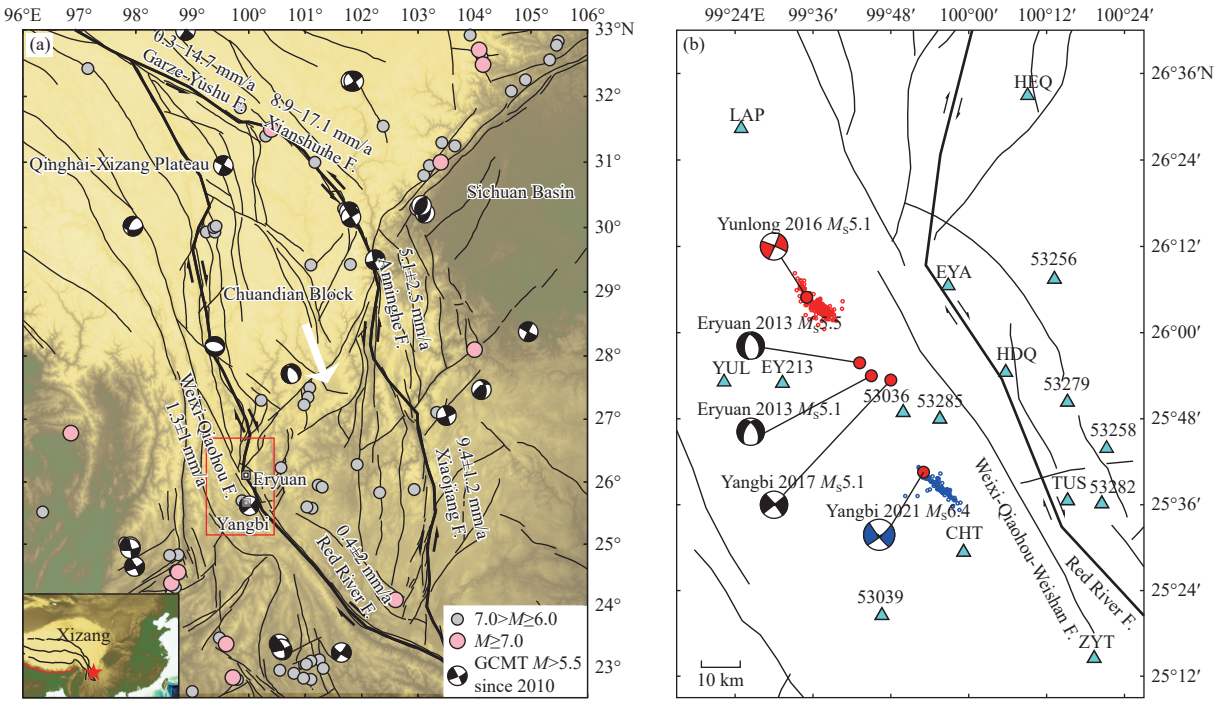

Figure 1. (a) The tectonic map and historical large earthquakes surrounding the study region. The pink and gray dots represent $M\geq$ 7.0 and 6.0 ≤ M<7.0 historical earthquakes, respectively. Inset map: The red star shows the location of study region. Black lines represent the structural sutures among blocks of Qinghai-Xizang Plateau. Red line marks the collision front between Indian and Eurasian plates. (b) The seismic stations (cyan triangles) and earthquake sequences near the Weixi-Qiaohou-Weishan Fault in western Yunnan.

investigated by deriving focal mechanisms of the mainshock and major aftershocks, which were used to depict the seismogenic fault (Jiang JZ et al., 2019). Based on relocated hypocenters and focal mechanisms, the seismogenic fault was suggested to be a NNE-striking blind or a sub-fault located between the NW-striking Weixi-Qiaohou Fault and Lancangjiang Fault (Jiang JZ et al., 2019). However, few studies have analyzed the foreshock patterns of the 2016 M_S5.1 Yunlong earthquake.

Although underlying physical mechanisms of earthquake nucleation processes and the role of foreshocks in the earthquake initiation process remain unclear, foreshocks may still provide unique and valuable information for the earthquake nucleation process. By studying the pattern of foreshocks and their relationship with the mainshock, we can better understand the underlying physics of earthquakes. In this study, we investigate the spatial-temporal pattern of 2016 M_S5.1 Yunlong foreshocks, and the stress perturbation of the largest foreshock, based on which the mechanism of mainshock nucleation is discussed. Besides, using the published catalog of 2017 and 2021 Yangbi earthquake sequences, we conduct an integrated analysis of time-dependent b values for the earthquake sequences in the region. The findings provide insights into the mechanisms of earthquake nucleation and the role of foreshocks in earthquake prediction.

2. Dataset and methods

2.1. Seismic data

Because of the great seismic hazard along the Red River fault in western Yunnan, multiple seismic networks have been deployed. The permanent stations of the China Array project were deployed with a spacing of ~40−60 km, while a temporal seismic array with a spacing of ~10−20 km has been launched since April 2011 (Wang BS et al., 2012; Yang HF et al., 2020). These stations recorded the 2016 M_S5.1 Yunlong earthquake rupture. We collected six months of continuous data (starting from November 2015) before the 2016 Yunlong mainshock from the China Earthquake Networks Center (CENC). A number of 16 stations within 80 km of the epicentral area were used for earthquake detection and location (Figure 1b).

2.2. Earthquake detection and location

To build a more complete earthquake catalog, we conducted earthquake detection using the matched filter detector. A number of 105 events in the CENC catalog were used as templates (Figure 2c), and then cross-

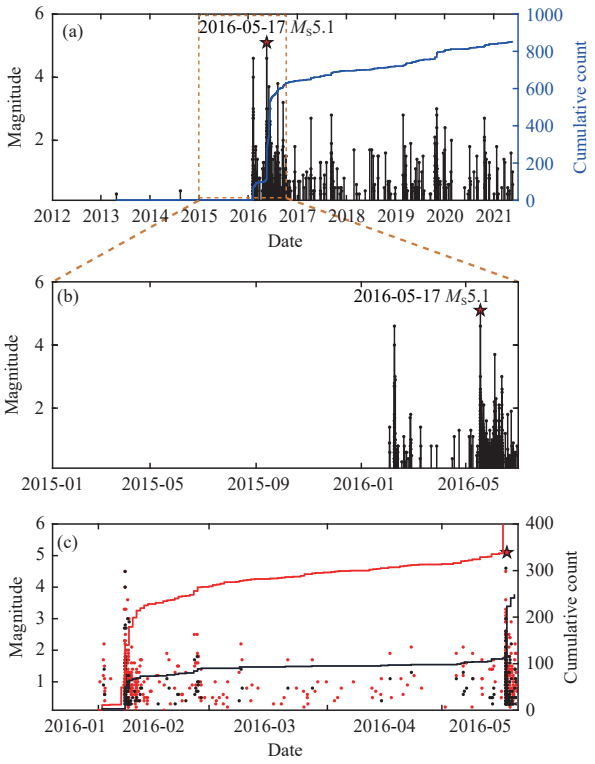

Figure 2. The temporal distribution of earthquake magnitude and cumulative count surrounding the 2016 Yunlong M_S5.1 earthquake (red star). The spatial region is the same as Figure 4a. The earthquakes were collected from CENC over the period from 2012 to 2021 (a) and from 2015-01 to 2016-05 (b). The blue curve represents the cumulative event count since 2012. (c) The comparison between the CENC catalog (black dots) and our catalog (red dots). The red and blue curves represent the cumulative count of events in our catalog and CENC since 2016-01, respectively.

correlated with continuous waveforms (Peng ZG and Zhao P, 2009; Yang H et al., 2009). The 3-component P waves (1.5 s before to 8 s after the P-wave arrival) were chosen as template waveforms. Following the processors in Zhu GH et al. (2022), a 1−20 Hz bandpass filter was adopted to improve the signal-to-noise ratio of the template and continuous data. A candidate earthquake was detected with a cross-correlation coefficient (CC) larger than 0.6 on one single station. If the original time of events detected by different template events was within 8 s, they were regarded as duplicate events. After removing the duplicate detections, we obtained 949 foreshocks with the initial locations as the same as their template events. The magnitude of detected events (M_{det})were calculated according to ratio (R) of maximum amplitudes between detected earthquakes and template earthquakes with magnitude (M_0) (Yang H et al., 2009; Zhu GH et al., 2019).

$$M_{det} = M_0 + \log_{10}(R). \quad (1)$$

We located the detected earthquakes using the Hypoinverse algorithm (Klein, 2002). The used 1D velocity model (Figure S1) was the same as Zhang YY et al. (2022), which was constructed from an active source velocity model at shallow depth and surface-wave tomography model for deep section. Double-difference method (hypoDD algorithm) was then used to improve the relative relocations (Waldhauser and Ellsworth, 2000). We obtained 7,104 P- and 3,287 S-phase differential time measurements from phase picks, and 76,790 P- and 4,650 S-phase differential times by cross-correlating P and S phases. We astricted a minimum number of 8 differential times per event pair and a maximum separation of 8 km. Eventually, we relocated 343 out of the detected foreshocks. A median relative location uncertainty was ~17 m laterally and ~25 m vertically in the hypoDD, but the actual location uncertainties are generally larger than that given by hypoDD inversion based on least-square criteria. A bootstrapping analysis was then adopted to compute the relocation uncertainty (Waldhauser and Ellsworth, 2000), giving a mean relocation uncertainty of 235 m laterally and 579 m vertically, respectively.

2.3. Repeating earthquake identification

Repeating earthquakes (or repeaters) are usually regarded as evidence for aseismic slip surrounding seismic fault patches (Kato et al., 2016; Nadeau and Johnson, 1998; Uchida and Bürgmann, 2019; Waldhauser and Schaff, 2021). However, it is challenging to recognize (Gao DW et al., 2021). In practice, the detection of repeaters mostly relies on the overlapping ratio of estimated earthquake source areas and/or the degree of waveform similarity (Uchida and Bürgmann, 2019; Waldhauser and Schaff, 2021).

We searched for possible repeating earthquakes, by calculating the maximum cross-correlation coefficient (CC) of seismograms of event pairs. We first tested the influence of filters on CC values. The 3-component seismograms of different events were filtered with a series of frequency bands (Figure 3), starting from 1.5 s before and 8 s after the P-wave arrival times. The CC values vary with different filter bands, showing a better waveform fitting at lower frequencies in general (Figure 3). Waveform similarity is affected by the filter band and epicentral distance, which is consistent with previous study (Gao DW et al., 2021). We adopted the criteria that the candidate repeater pairs have at least one CC ≥ 0.95 and a mean of five highest CC >0.9 (Waldhauser and Schaff, 2021). Using typical filter bands of 1−10 Hz or 1−20 Hz for identifying repeating events, no event pairs meet the criteria. The event pair with the highest CC value among

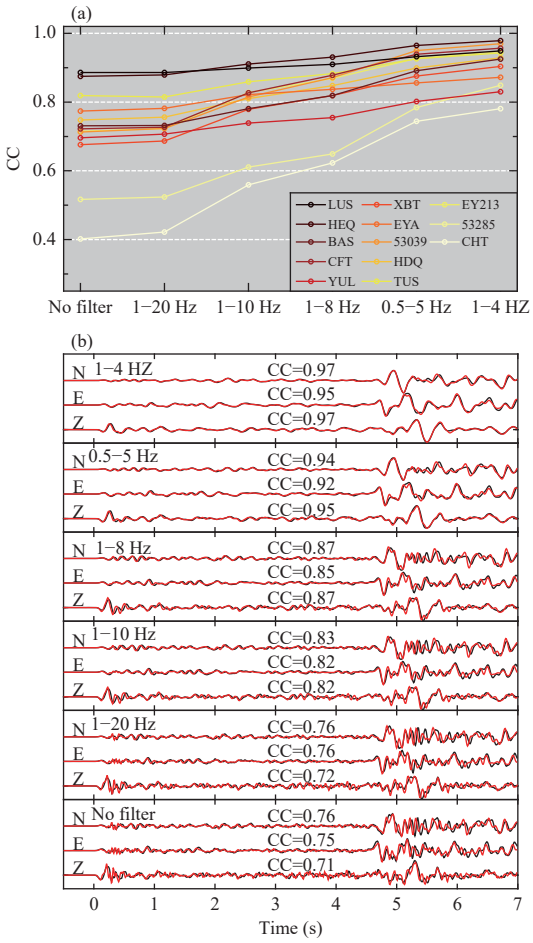

Figure 3. Cross-correlation coefficients (CC) of waveforms between two different events. (a) Effects of filters and epicentral distance on CC of waveforms. The curves are colored by epicentral distances. (b) Normalized example 3-component waveforms of an event pair on 53,039 station with different filters aligned at the P-phase arrival.

the 2016 Yunlong foreshocks is shown in Figure 3.

2.4. Source parameter inversion and Coulomb failure stress (CFS) changes

Focal mechanism solutions of the largest foreshock were derived from the Cut-And-Paste (CAP) method (Zhao LS and Helmberger, 1994; Zhu LP and Helmberger, 1996). The CAP method adopts a grid search approach in the source parameter domain (strike, dip, rake, and centroid depth) to find the best fitting between the synthetic and observed seismograms (Figures S2 and S3). The synthetic seismograms were calculated using the 1D velocity model through the frequency-wavenumber integration method (Zhu LP and Rivera, 2002). During the inversion, the body and surface waveforms were filtered in the frequency band of 0.05–0.2 and 0.03–0.1 Hz, respectively, and were allowed for separate time shifts to alleviate bias caused by inaccurate velocity model.

To explore the relationship between foreshocks and mainshock, we calculated the CFS of the largest M_S4.5 foreshock of the 2016 Yunlong earthquake using the Coulomb 3.3 package (Lin J and Stein, 2004; Toda et al., 2005). The parameters were set as follows: Poisson's ratio = 0.25, coefficient of friction = 0.5, and Young's modulus = 8×10^4 MPa. The NW-trending distribution of the 2016 Yunlong seismicity, the nearby major known faults, and other earthquake sequences (including the 2021 M_S6.4 Yangbi sequence and 2013 Yunlong earthquake swarm) are dominantly in the NW-trending direction. Therefore, we regarded the NW-trending fault plane as the preferred one, and the source fault was derived from moment tensor inversion with (strike, dip, rake) = (324°, 84°, −141°). Considering the possibility of different rupture faults (e.g., Long F et al., 2021), we also calculated the CFS with the other nodal plane (strike, dip, rake) = (229°, 51°, −8°). The receiver fault is set to be the same as the mainshock rupture derived from moment tensor inversion with (strike, dip, rake) = (293°, 86°, 177°).

2.5. Temporal changes in *b* value

To investigate the statistical features of the foreshock sequences in the study region, we collected the published catalog of earthquake sequences with mainshock magnitude M_S>5. Another two M_S>5 earthquakes (2017 M_S5.1 and 2021 M_S6.4 Yangbi earthquakes) in the region have been recorded with foreshocks by previous studies (e.g., Li J et al., 2020; Zhu GH et al., 2022). We collected the events catalog of the 2017 Yangbi earthquakes built by Li J et al. (2020) using matched filter detection. For the 2021 Yangbi earthquake sequence, we used the events catalog built by Zhu GH et al. (2022) using machine learning and matched filter methods.

The *b* value and its temporal changes were estimated based on the published catalogs using ZMAP (Wiemer, 2001). Because of the concentrated spatial distribution (Figure 1b), we didn't conduct spatial partitioning for each foreshock sequence. To avoid the bias caused by the mainshock, we divided the event sequences into two parts: a pre- and a post-mainshock catalog. We also removed the events immediately following the mainshocks, which are likely incomplete and heterogeneous (Gulia and Wiemer, 2019). For *b* value estimation of pre-mainshock catalog, we used the sliding window length (sample size) of 100 events, with 10 events overlapping. For *b* value estimation of post-mainshock catalog, we increase the sliding window length of 200 events, because aftershock sequences are data-rich. The transient *b* values were computed using the maximum-curvature method with a magnitude bin of 0.1

(Wiemer and Wyss, 2000). Uncertainties of *b* values were computed by bootstrapping. We then estimated the background *b* value using seismicity reported by the CENC catalog (Figure S4). The earthquakes in the same spatial region as Figure 1b were chosen for calculating the background *b* value.

3. Results

A total of 949 foreshocks were identified using matched filter detection, but many of them generated clear signals on only a few nearest stations. Eventually, 343 of them with a magnitude of −0.8−4.5 were relocated, depicting a SE-trending fault (Figure 4a). Most earthquakes occurred at depths ranging from 2−15 km (Figure 4b). The focal depth of the mainshock was 8.5 km.

The seismic activity significantly increased since Feb 1, 2016, with the largest foreshock M_S4.5 occurring on Feb 7, about 3 months before the mainshock (Figures 2 and 5a). The Yunlong sequence started with a magnitude 1.0 foreshock that occurred ~5.5 km southeast of the M_S5.1 mainshock (Figures 5a and 5b). In the following days, most foreshocks ruptured the adjacent area of the first event at the southeastern fault zone, where the largest foreshock occurred (Figure 5b). There were also several foreshocks ruptured the northwestern fault zone where the mainshock nucleated. The largest M_S4.5 foreshock in the Yunlong sequence was located ~5.2 km away from the mainshock's hypocenter in the southeast direction. Immediately following the largest foreshock, many earthquakes with smaller magnitudes dispersively occurred along the entire fault zone (Figure 5). The rate of seismic events obviously increased immediately following the largest M_S4.5 foreshock, but then gradually decreased with time until the occurrence of mainshock (Figures 5a and Figure S5). Overall, the spatial-temporal evolution of seismicity exhibited no localization or systematic migration towards the mainshock.

The largest foreshock and the 2016 Yunlong mainshock showed a similar strike-slip faulting mechanism (Figure 5). The foreshocks and the mainshock hypocenter roughly delineated an NW-trending fault, in accord with the NW-trending nodal plane of the focal mechanisms (Figure 5). Therefore, the NW-trending nodal plane was regarded as the preferred fault. The largest M_S4.5 foreshock of the 2016 Yunlong earthquake increased Coulomb stress of ~0.3 bar at the hypocenter of mainshock (Figure 6a). Similarly, for the 2021 Yangbi M_S6.4 earthquake sequence, the largest M_S5.3 foreshock increased the Coulomb stress by 0.5 bar at the mainshock hypocenter, and cumulative shear stress of previous major foreshocks increased of 2.2−10.1 bar (based on different source models) at the mainshock hypocenter (Zhu GH et al., 2022). Therefore, the 2016 Yunlong and 2021 Yangbi earthquakes may indicate stress triggering of the mainshock.

Statistical characteristics of three foreshock sequences (2016 Yunlong, 2017 Yangbi, and 2021 Yangbi) in the region were examined. Due to a limited number of relocated foreshocks of the 2016 M_S5.1 Yunglong sequence, we were unable to calculate the transient *b* values. For the 2017 and 2021 Yangbi earthquake sequences, the transient

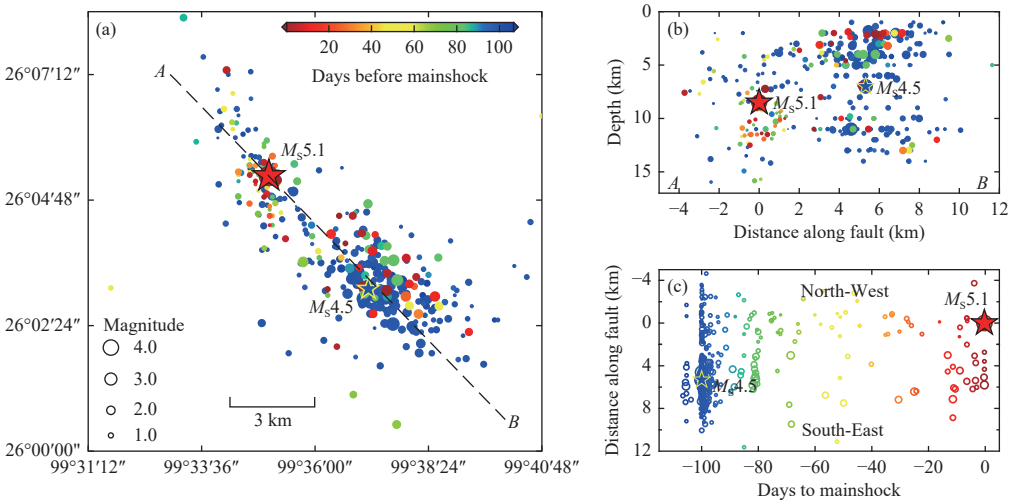

Figure 4. Spatial-temporal evolution of the Yunlong foreshocks. The events were colored by the original time relative to the mainshock in the map view (a), cross-section view (b) and spatial-temporal evolution along cross-section *AB* (c). The red star marks the mainshock, and the blue star with yellow frame marks the largest M_S4.5 foreshock. The distance in (b) and (c) is taken along the fault strike direction with 0 km corresponding to the mainshock hypocenter.

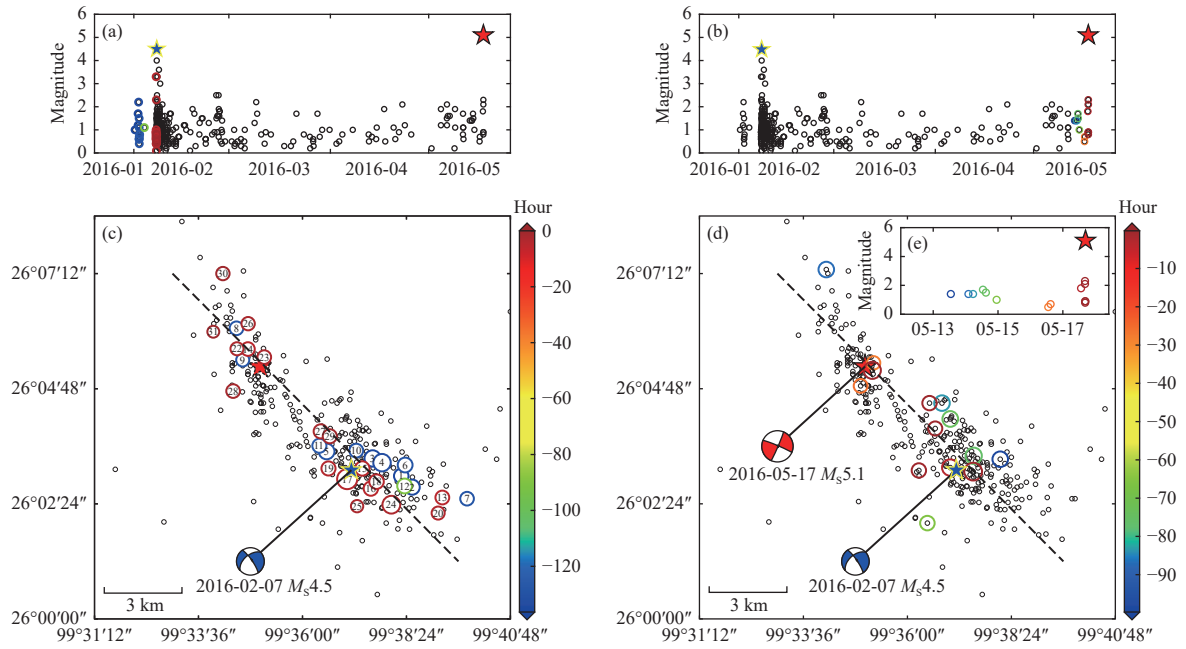

Figure 5. Spatial-temporal evolution of the Yunlong foreshock sequence colored by their original time relative to the largest M_S4.5 foreshock (a, b), and relative to the mainshock (c, d), respectively. The earthquakes are numbered according to the order of the original time. The circle size is scaled by the magnitude. The red and blue stars mark the epicenter of the mainshock and the largest foreshock.

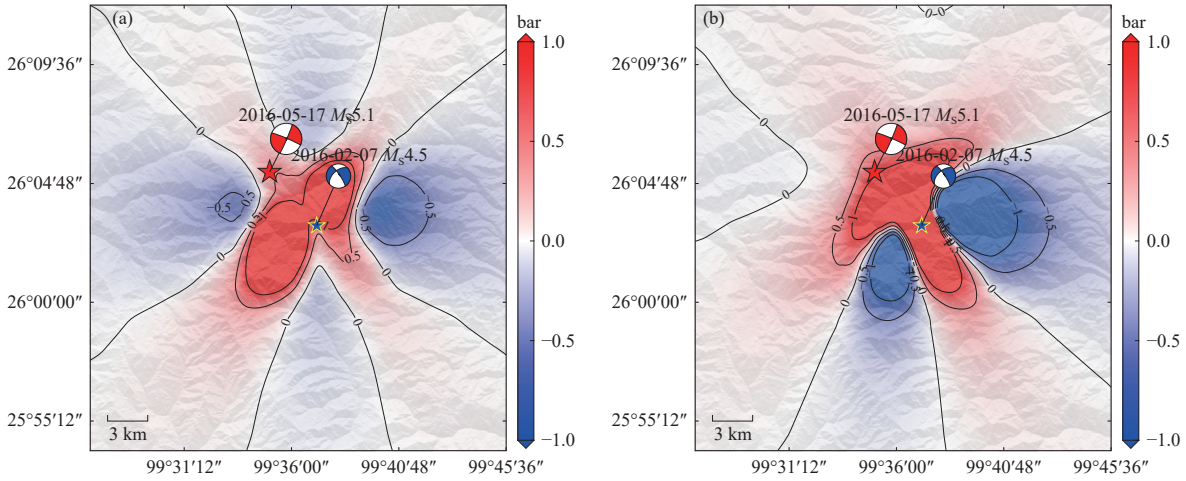

Figure 6. The calculated Coulomb failure stress caused by the largest M_S 4.5 foreshock at the mainshock focal depth with (a) NW- (324°) and (b) NE-trending (229°) fault plane, respectively. The red (blue) colors indicate positive (negative) stress changes. The red and blue stars mark the epicenter of the mainshock and the largest foreshock, respectively.

b values were estimated (Figure 7). An obvious decrease in *b* values before the mainshocks was observed before the 2017 and 2021 Yangbi mainshocks (Figure 7). The estimated background *b* value is 0.73 (Figure S3).

4. Discussion

Numerical modeling and laboratory experiments have found signals of slip acceleration before rapid seismic rupture, companying with accelerating foreshock activities (Ampuero and Rubin, 2008; Marty et al., 2023; McLaskey, 2019; McLaskey and Kilgore, 2013; Ohnaka and Shen LF, 1999). A phase of pre-slip accelerating into dynamic rupture is also suggested by natural observations (Tape et al., 2018). Moreover, the localizing foreshocks preceding a mainshock are also evidenced in nature, varying from a few days (Savage et al., 2017) to several years (Ben-Zion and Zaliapin, 2020). However, our observed spatial-

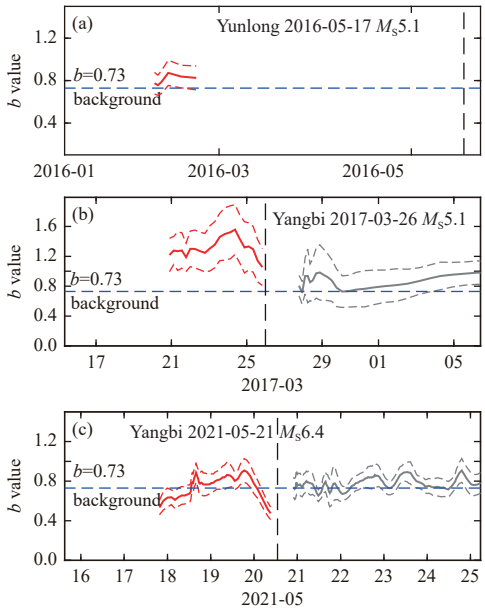

Figure 7. The estimated transient *b* values of the three earthquake sequences. The solid curves represent *b* values with uncertainties marked by dashed curves. The red and grey colors show estimates for foreshocks and aftershocks, respectively. The vertical dashed black lines mark the time of mainshocks. The dashed blue lines stand for calculated background *b* values.

temporal evolution patterns of the Yunlong foreshocks exhibit a random pattern, rather than a localization or systematic migration towards the mainshock. There are no repeating earthquakes of foreshock occurrence either, which obviously differs from a nucleation-related pre-slip model. In addition, fluids are suggested to play a critical role in the 2013 Yunlong earthquake swarm (Liu M et al., 2023). However, the spatial-temporal pattern of the 2016 Yunlong and 2021 Yangbi earthquakes didn't show a fluid-triggered parabola front. Instead, the stress-triggering mechanism among foreshocks and mainshock is supported by our observations of the Yunlong sequence.

The Coulomb failure stress changes caused by the largest foreshock is ~0.3 bar at the mainshock's hypocenter. A critical triggering value may vary from site to site and can be lower than ~0.1 bar according to previous studies (Freed, 2005; Ziv and Rubin, 2000). For example, Ziv and Rubin (2000) investigated cumulative static stress changes imposed on 63 M>4.5 earthquakes in central California, and suggested that 70% of the cumulative stress changes at the time of rupture increase values of <0.1 bar and <0.01 bar. Furthermore, there are many small earthquakes between the largest foreshock and mainshock, which may facilitate stress transfers between earthquakes (Helmstetter et al., 2005). Although the stress changes caused by small earthquakes cannot be calculated in this study, they may accumulate and increase stress changes at the mainshock's hypocenter (Helmstetter et al., 2005; Zhu GH et al., 2022).

Our analyses suggest a cascade-triggering mechanism for foreshock sequences in western Yunnan, which seems pessimistic for earthquake forecasting. However, on the other hand, an obvious decrease in *b* values before the mainshocks was observed for the 2017 and 2021 Yangbi foreshocks, although the change in *b* values of the Yunlong sequence is unidentified due to the limited number of foreshocks. Besides, a reduction in *b* values before mainshock has also been documented in other Yunnan regions. For example, a recent study of statistical seismicity features shows *b* value reduction for foreshock sequences 2014 M_S6.1 Yingjiang, Yunnan, earthquake sequence (Li L et al., 2024).

The *b* value abruptly decreases before the mainshocks, which is likely related to stress increase before the mainshock (Scholz, 1968). However, the reported precursory decrease in *b* values varies significantly in time scale: from a decadal scale decrease documented in the 2011 Tohoku main slip area (Nanjo et al., 2012), to a gradual decrease three years before the 2014 Iquique earthquake (Schurr et al., 2014), to a sudden drop ten days before the 2009 L'Aquila mainshock (Gulia et al., 2016). Obvious changes in *b* values relative to background values before large events were established as a traffic-light system for earthquake warnings, which could assess whether the mainshock has already happened or is yet to come (Gulia and Wiemer, 2019). Such observations can contribute to improving probabilistic short-term forecasting models in the region, but the challenge of real-time warning stems from the uncertain time scale of drops in *b* values.

5. Summary

By investigating the spatio-temporal evolution and source parameters of the 2016 Yunglong earthquake sequence in western Yunnan, China, we discussed their implications for the earthquake nucleation processes in the region. The scattered spatial pattern of foreshocks in the region differs from the features of a pre-slip earthquake nucleation process. Rather, the 2016 Yunlong can be well explained by stress triggering. We also examine the time-dependent *b* values of the major earthquakes with recorded foreshocks in the neighboring region, including the 2017 and 2021 Yangbi earthquakes. Although the earthquakes in this region exhibit a cascade process, the established temporal transient in *b* values shows precursory drops,

which is optimistic for probabilistic short-term hazard warnings in the region.

Data and Resources

Supplementary material of figures related to this article can be found online. The seismic waveforms and earthquake catalog produced in this study can be accessed by connecting with the corresponding author. The fault lines in western China are obtained from the HimaTibet-Map-1.1 database (Styron et al., 2010).

Acknowledgments

We thank two anonymous reviewers for their constructive comments. We appreciate the scientists and technicists who maintain the seismic networks. This study is supported by the Laoshan Laboratory project (LSKJ202204100), National Natural Science Foundation of China (Nos. U2344221, 92158205, 42406064), Hong Kong Research Grant Council Grants (14306122), the Taishan Scholar Foundation of Shandong Province (tstp20230638), and Shandong Province Outstanding Youth Science Fund Project Overseas (2023HWYQ-099). The figures were plotted using the GMT tools (Wessel et al., 2013).

Conflict of interest

Hongfeng Yang serves as an editor-in-chief for Earthquake Science and was not involved in the editorial review or the decision-making process for this article. All authors declare that they have no competing interests.

References

Abercrombie RE and Mori J (1996). Occurrence patterns of foreshocks to large earthquakes in the western United States. Nature **381**(6580): 303–307. https://doi.org/10.1038/381303a0.

Ampuero JP and Rubin AM (2008). Earthquake nucleation on rate and state faults – Aging and slip laws. J Geophys Res: Solid Earth **113**(B1): B01302. https://doi.org/10.1029/2007jb005082.

Ben-Zion Y and Zaliapin I (2020). Localization and coalescence of seismicity before large earthquakes. Geophys J Int **223**(1): 561–583. https://doi.org/10.1093/gji/ggaa315.

Bouchon M, Karabulut H, Aktar M, Özalaybey S, Schmittbuhl J and Bouin MP (2011). Extended nucleation of the 1999 M_W7.6 Izmit earthquake. Science **331**(6019): 877–880. https://doi.org/10.1126/science.1197341.

Cattania C and Segall P (2021). Precursory slow slip and foreshocks on rough faults. J Geophys Res: Solid Earth **126**(4): e2020JB020430. https://doi.org/10.1029/2020jb020430.

Chen YT, Gu HD and Lu ZX (1980). Variations of gravity before and after the Haicheng earthquake, 1975 and the Tangshan earthquake, 1976. Acta Seismol Sin **2**(1): 21–31. (in Chinese with English abstract).

Dascher-Cousineau K, Lay T and Brodsky EE (2020). Two foreshock sequences Post Gulia and Wiemer (2019). Seismol Res Lett **91**(5): 2843–2850. https://doi.org/10.1785/0220200082.

Ellsworth WL and Bulut F (2018). Nucleation of the 1999 Izmit earthquake by a triggered cascade of foreshocks. Nat Geosci **11**(7): 531–535. https://doi.org/10.1038/s41561-018-0145-1.

Ellsworth WL (2019). From foreshocks to mainshocks: mechanisms and implications for earthquake nucleation and rupture propagation. In: Bizzarri A, Das S and Petri A eds. Proceedings of the International School of Physics "Enrico Fermi": Volume 202: Mechanics of Earthquake Faulting. IOS Press, Amsterdam, pp. 95–112. https://doi.org/10.3254/978-1-61499-979-9-95.

Freed AM (2005). Earthquake triggering by static, dynamic and postseismic stress transfer. Annu Rev Earth Planet Sci **33**(1): 335–367. https://doi.org/10.1146/annurev.earth.33.092203.122505.

Gao DW, Kao H and Wang B (2021). Misconception of waveform similarity in the identification of repeating earthquakes. Geophys Res Lett **48**(13): e2021GL092815. https://doi.org/10.1029/2021gl092815.

Goebel THW, Schorlemmer D, Becker TW, Dresen G and Sammis CG (2013). Acoustic emissions document stress changes over many seismic cycles in stick-slip experiments. Geophys Res Lett **40**(10): 2049–2054. https://doi.org/10.1002/grl.50507.

Gulia L, Tormann T, Wiemer S, Herrmann M and Seif S (2016). Short-term probabilistic earthquake risk assessment considering time-dependent *b* values. Geophys Res Lett **43**(3): 1100–1108. https://doi.org/10.1002/2015GL066686.

Gulia L and Wiemer S (2019). Real-time discrimination of earthquake foreshocks and aftershocks. Nature **574**(7777): 193–199. https://doi.org/10.1038/s41586-019-1606-4.

Gutenberg B and Richter CF (1944). Frequency of earthquakes in California. Bull Seismol Soc Am **34**(4): 185–188. https://doi.org/10.1785/BSSA0340040185.

He X, Zhao LF, Xie XB, Zhang L and Yao ZX (2023). Eastward expansion of the Tibetan plateau: Insights from stress drops of the 2021 M_S6.4 Yangbi, Yunnan and M_S7.4 Maduo, Qinghai earthquake sequences in China. Front Earth Sci **11**: 1081605. https://doi.org/10.3389/feart.2023.1081605.

Helmstetter A, Kagan YY and Jackson DD (2005). Importance of small earthquakes for stress transfers and earthquake triggering. J Geophys Res: Solid Earth **110**(B5): B05S08. https://doi.org/10.1029/2004jb003286.

Huang H, Meng LS, Bürgmann R, Wang W and Wang K (2020). Spatio-temporal foreshock evolution of the 2019 *M*6.4 and *M*7.1 Ridgecrest, California earthquakes. Earth Planet Sci Lett **551**: 116582. https://doi.org/10.1016/j.epsl.2020.1165

82.

Jiang JZ, Li J and Fu H (2019). Seismicity analysis of the 2016 M_S5.0 Yunlong Earthquake, Yunnan, China and its tectonic implications. Pure Appl Geophys **176**(3): 1225–1241. https://doi.org/10.1007/s00024-018-2067-7.

Jin AS and Aki K (1986). Temporal change in coda *Q* before the Tangshan Earthquake of 1976 and the Haicheng Earthquake of 1975. J Geophys Res: Solid Earth **91**(B1): 665–673. https://doi.org/10.1029/JB091iB01p00665.

Jones LM, Wang BQ, Xu SX and Fitch TJ (1983). The foreshock sequence of the February 4, 1975, Haicheng earthquake (*M*=7.3). Acta Seismol Sin **5**(1): 1–14. (in Chinese with English abstract).

Kato A, Obara K, Igarashi T, Tsuruoka H, Nakagawa S and Hirata N (2012). Propagation of slow slip leading up to the 2011 M_W9.0 Tohoku-Oki earthquake. Science **335**(6069): 705–708. https://doi.org/10.1126/science.1215141.

Kato A and Nakagawa S (2014). Multiple slow-slip events during a foreshock sequence of the 2014 Iquique, Chile M_W8.1 earthquake. Geophys Res Lett **41**(15): 5420–5427. https://doi.org/10.1002/2014GL061138.

Kato A, Fukuda J, Kumazawa T and Nakagawa S (2016). Accelerated nucleation of the 2014 Iquique, Chile M_W8.2 Earthquake. Sci Rep **6**(1): 24792. https://doi.org/10.1038/srep24792.

Klein FW (2002). User's guide to HYPOINVERSE-2000, a Fortran program to solve for earthquake locations and magnitudes. U. S. Geological Survey, Menlo Park. https://doi.org/10.3133/ofr02171.

Lei XL, Wang ZW, Ma SL and He CR (2021). A preliminary study on the characteristics and mechanism of the May 2021 M_S6.4 Yangbi earthquake sequence, Yunnan, China. Acta Seismol Sin **43**(3): 261–286 . https://doi.org/10.11939/jass.20210100 (in Chinese with English abstract).

Lei XL, Wang ZW, Ma SL and He CR (2024). Step-over of strike-slip faults and overpressure fluid favor occurrence of foreshocks: Insights from the 1975 Haicheng fore-main-aftershock sequence, China. Earthq Res Adv **4**(1): 100237. https://doi.org/10.1016/j.eqrea.2023.100237.

Li J, Jiang JZ and Yang JQ (2020). Microseismic detection and relocation of the 2017 M_S4.8 and M_S5.1 Yangbi earthquake sequence, Yunnan. Acta Seismol Sin **42**(5): 527–542. https://doi.org/10.11939/jass.20190161 (in Chinese with English abstract).

Li L, Wang BS, Peng ZG, Hou JX and Wang F (2024). Statistical features of seismicity associated with large earthquakes on the Chinese continent between 2008 and 2019 based on newly detected catalogs. Seismol Res Lett **95**(3): 1701–1717. https://doi.org/10.1785/0220230189.

Lin J and Stein RS (2004). Stress triggering in thrust and subduction earthquakes and stress interaction between the southern San Andreas and nearby thrust and strike-slip faults. J Geophys Res: Solid Earth **109**(B2): B02303. https://doi.org/10.1029/2003jb002607.

Liu M, Li HY, Li L, Zhang M and Wang WT (2022). Multistage nucleation of the 2021 Yangbi M_S6.4 Earthquake, Yunnan, China and its foreshocks. J Geophys Res: Solid Earth **127**(5): e2022JB024091. https://doi.org/10.1029/2022jb024091.

Liu M, Li L, Zhang M, Lei XL, Nedimović MR, Plourde AP, Guo RM, Wang WT and Li HY (2023). Complexity of initiation and evolution of the 2013 Yunlong earthquake swarm. Earth Planet Sci Lett **612**: 118168. https://doi.org/10.1016/j.epsl.2023.118168.

Long F, Qi YP, Yi GX, Wu WW, Wang GM, Zhao XY, Peng GL (2021). Relocation of the M_S6.4 Yangbi earthquake sequence on May 21, 2021 in Yunnan Province and its seismogenic structure analysis. Chin J Geophys **64**(8): 2631–2646 . https://doi.org/10.6038/cjg2021O0526 (in Chinese with English abstract).

Marty S, Schubnel A, Bhat HS, Aubry J, Fukuyama E, Latour S, Nielsen S and Madariaga R (2023). Nucleation of laboratory earthquakes: Quantitative analysis and scalings. J Geophys Res: Solid Earth **128**(3): e2022JB026294. https://doi.org/10.1029/2022jb026294.

McLaskey GC and Kilgore BD (2013). Foreshocks during the nucleation of stick-slip instability. J Geophys Res: Solid Earth **118**(6): 2982–2997. https://doi.org/10.1002/jgrb.50232.

McLaskey GC (2019). Earthquake initiation from laboratory observations and implications for foreshocks. J Geophys Res: Solid Earth **124**(12): 12882–12904. https://doi.org/10.1029/2019jb018363.

Mori J (1996). Rupture directivity and slip distribution of the *M*4.3 foreshock to the 1992 Joshua Tree earthquake, Southern California. Bull Seismol Soc Am **86**(3): 805–810. https://doi.org/10.1785/bssa0860030805.

Nadeau RM and Johnson LR (1998). Seismological studies at Parkfield VI: Moment release rates and estimates of source parameters for small repeating earthquakes. Bull Seismol Soc Am **88**(3): 790–814. https://doi.org/10.1785/BSSA0880030790.

Nanjo KZ, Hirata N, Obara K and Kasahara K (2012). Decade-scale decrease in *b* value prior to the *M*9-class 2011 Tohoku and 2004 Sumatra quakes. Geophys Res Lett **39**(20): L20304. https://doi.org/10.1029/2012GL052997.

Ohnaka M and Shen LF (1999). Scaling of the shear rupture process from nucleation to dynamic propagation: Implications of geometric irregularity of the rupturing surfaces. J Geophys Res: Solid Earth **104**(B1): 817–844. https://doi.org/10.1029/1998jb900007.

Peng ZG and Zhao P (2009). Migration of early aftershocks following the 2004 Parkfield earthquake. Nat Geosci **2**(12): 877–881. https://doi.org/10.1038/ngeo697.

Peng ZG, Lei XL, Wang QY, Wang D, Mach P, Yao DD, Kato A, Obara K and Campillo M (2024). The evolution process between the earthquake swarm beneath the Noto Peninsula, Central Japan and the 2024 *M*7.6 Noto Hanto earthquake sequence. Earthq Res Adv. https://doi.org/10.1016/j.eqrea.2024.100332(查阅网上资料,未找到卷期页码信息,请补充).

Savage HM, Keranen KM, Schaff DP and Dieck C (2017). Possible precursory signals in damage zone foreshocks. Geophys Res Lett **44**(11): 5411–5417. https://doi.org/10.1002/2017gl073226.

Scholz CH (1968). The frequency-magnitude relation of

microfracturing in rock and its relation to earthquakes. Bull Seismol Soc Am **58**(1): 399–415. https://doi.org/10.1785/BSSA0580010399.

Scholz CH (1977). A physical interpretation of the Haicheng earthquake prediction. Nature **267**(5607): 121–124. https://doi.org/10.1038/267121a0.

Schurr B, Asch G, Hainzl S, Bedford J, Hoechner A, Palo M, Wang RJ, Moreno M, Bartsch M, Zhang Y, Oncken O, Tilmann F, Dahm T, Victor P, Barrientos S and Vilotte JP (2014). Gradual unlocking of plate boundary controlled initiation of the 2014 Iquique earthquake. Nature **512**(7514): 299–302. https://doi.org/10.1038/nature13681.

Shapiro SA, Huenges E and Borm G (1997). Estimating the crust permeability from fluid-injection-induced seismic emission at the KTB site. Geophys J Int **131**(2): F15–F18. https://doi.org/10.1111/j.1365-246X.1997.tb01215.x.

Tape C, Holtkamp S, Silwal V, Hawthorne J, Kaneko Y, Ampuero JP, Ji C, Ruppert N, Smith K and West ME (2018). Earthquake nucleation and fault slip complexity in the lower crust of central Alaska. Nat Geosci **11**(7): 536–541. https://doi.org/10.1038/s41561-018-0144-2.

Toda S, Stein RS, Richards-Dinger K and Bozkurt SB (2005). Forecasting the evolution of seismicity in southern California: Animations built on earthquake stress transfer. J Geophys Res **110**(B5): B05S16. https://doi.org/10.1029/2004jb003415.

Uchida N and Bürgmann R (2019). Repeating earthquakes. Annu Rev Earth Planet Sci **47**(1): 305–332. https://doi.org/10.1146/annurev-earth-053018-060119.

Waldhauser F and Ellsworth WL (2000). a double-difference earthquake location algorithm: Method and application to the Northern Hayward Fault, California. Bull Seismol Soc Am **90**(6): 1353–1368. https://doi.org/10.1785/0120000006.

Waldhauser F and Schaff DP (2021). A comprehensive search for repeating earthquakes in Northern California: Implications for fault creep, slip rates, slip partitioning and transient stress. J Geophys Res: Solid Earth **126**(11): e2021JB022495. https://doi.org/10.1029/2021jb022495.

Wang BS, Ge HK, Yang W, Wang WT, Wang B, Wu GH and Su YJ (2012). Transmitting seismic station monitors fault zone at depth. EoS, Trans AGU **93**(5): 49–50. https://doi.org/10.1029/2012EO050001.

Wang KL, Chen QF, Sun SH and Wang AD (2006). Predicting the 1975 Haicheng earthquake. Bull Seismol Soc Am **96**(3): 757–795. https://doi.org/10.1785/0120050191.

Wessel P, Smith WHF, Scharroo R, Luis J and Wobbe F (2013). Generic mapping tools: Improved version released. Eos, Trans AGU **94**(45): 409–410. https://doi.org/10.1002/2013eo450001.

Wiemer S and Wyss M (2000). Minimum magnitude of completeness in earthquake catalogs: Examples from Alaska, the Western United States and Japan. Bull Seismol Soc Am **90**(4): 859–869. https://doi.org/10.1785/0119990114.

Wiemer S (2001). A software package to analyze seismicity: ZMAP. Seismol Res Lett **72**(3): 373–382. https://doi.org/10.1785/gssrl.72.3.373.

Xu SX, Wang BQ, Jones LM, Ma XF and Shen PW (1982). The foreshock sequence of haicheng earthquake and earthquake swarm —the use of foreshock sequences in earthquake prediction. Tectonophysics **85**(1-2): 91–105. https://doi.org/10.1016/0040-1951(82)90079-8.

Yang H, Zhu L and Chu R (2009). Fault-plane determination of the 18 April 2008 Mount Carmel, Illinois, Earthquake by detecting and relocating aftershocks. Bull Seismol Soc Am **99**(6): 3413–3420. https://doi.org/10.1785/0120090038.

Yang HF, Duan YH, Song JH, Jiang XH, Tian XF, Yang W, Wang WT and Yang J (2020). Fine structure of the Chenghai Fault Zone, Yunnan, China, constrained from teleseismic travel time and ambient noise tomography. J Geophys Res: Solid Earth **125**(7): e2020JB019565. https://doi.org/10.1029/2020jb019565.

Yoon CE, Yoshimitsu N, Ellsworth WL and Beroza GC (2019). Foreshocks and mainshock nucleation of the 1999 M_W7.1 Hector Mine, California, Earthquake. J Geophys Res: Solid Earth **124**(2): 1569–1582. https://doi.org/10.1029/2018jb016383.

Zhang YY, An YR, Long F, Zhu GH, Qin M, Zhong YS, Xu Q and Yang HF (2022). Short-term foreshock and aftershock patterns of the 2021 M_S6.4 Yangbi Earthquake sequence. Seismol Res Lett **93**(1): 21–32. https://doi.org/10.1785/0220210154.

Zhao LS and Helmberger DV (1994). Source estimation from broadband regional seismograms. Bull Seismol Soc Am **84**(1): 91–104. https://doi.org/10.1785/BSSA0840010091.

Zhou YJ, Ren CM, Ghosh A, Meng HR, Fang LH, Yue H, Zhou SY and Su YJ (2022). Seismological characterization of the 2021 Yangbi foreshock-mainshock sequence, Yunnan, China: More than a triggered cascade. J Geophys Res: Solid Earth **127**(8): e2022JB024534. https://doi.org/10.1029/2022jb024534.

Zhu GH, Yang HF, Lin J, Zhou ZY, Xu M, Sun JL and Wan KY (2019). Along-strike variation in slab geometry at the southern Mariana subduction zone revealed by seismicity through ocean bottom seismic experiments. Geophys J Int **218**(3): 2122–2135. https://doi.org/10.1093/gji/ggz272.

Zhu GH, Yang HF, Tan YJ, Jin MP, Li XB and Yang W (2022). The cascading foreshock sequence of the M_S6.4 Yangbi earthquake in Yunnan, China. Earth Planet Sci Lett 591: 117594. https://doi.org/10.1016/j.epsl.2022.117594.

Zhu LP and Helmberger DV (1996). Advancement in source estimation techniques using broadband regional seismograms. Bull Seismol Soc Am **86**(5): 1634–1641. https://doi.org/10.1785/BSSA0860051634.

Zhu LP and Rivera LA (2002). A note on the dynamic and static displacements from a point source in multilayered media. Geophys J Int **148**(3): 619–627. https://doi.org/10.1046/j.1365-246X.2002.01610.x.

Ziv A and Rubin AM (2000). Static stress transfer and earthquake triggering: No lower threshold in sight? J Geophys Res: Solid Earth **105**(B6): 13631–13642. https://doi.org/10.1029/2000jb900081.